Journal of Sound and Vibration (2002) **257**(1), 177–188
doi:10.1006/jsvi.2001.4229, available online at http://www.idealibrary.com on IDEAL®

LETTERS TO THE EDITOR

EFFECTS OF VISCOUS FRICTION AND NON-FRICTION DAMPING MECHANISMS IN A RECIPROCATING ENGINE

Y. Wang and T. C. Lim

Department of Mechanical Engineering, 290 *Hardaway Hall*, *Box* 870276, *The University of Alabama*, *Tuscaloosa*, *AL* 35487-0276, *U.S.A. E-mail*: *tlim@coe.eng.ua.edu*

(*Received* 20 *December* 2001)

1. INTRODUCTION

Reciprocating engines are widely used in automotive, aerospace and industrial applications. One of the critical concerns is the inherent torsional resonances in the system. The ability to quantity these natural mode response more precisely also requires a better understanding of the damping characteristics. In a early experimental study by Wang and Lim [1], the torsional damping coefficients in typical reciprocating engines were shown to vary with crank angle position (and thus time as well) similar to the predicted quasi-static natural frequency function but opposite to the effective mass moment of inertia trend. A second study [2] analyzed the major sources of modal damping, and concluded that the connecting rod–crank pin component contributed most significantly to the variation observed. To further understand the underlying cause of damping variation, various form of dissipative mechanisms in a reciprocating engine are examined here.

There are several known basic forms of damping-producing mechanisms, namely sliding, pure rolling, and cyclical lateral/tilting motion, in a reciprocating engine. The first two forms are of the viscous friction type due to simple shear resistance in the oil film, while the third one may be a combination of oil film resistance to compressive displacement and impactive types. Even though much studies on reciprocating engine vibration have been conducted previously as noted by Ker Wilson [3], the actual contributions to torsional damping are still not quantified conclusively. In fact, earlier calculations showed that viscous friction cannot account for the bulk of the measured vibratory energy dissipation. In some cases, the variations of excitation frequency due to speed fluctuation, known as *apparent damping* for its detuning effect, were thought to be the key to the additional damping observed. In other case, the *apparent damping* due to cyclical fluctuation in the natural frequency as the result of variation of the effective mass moment of inertia term was assumed to be the source of damping. However, further investigations [3] concluded that their contributions to the reduction of the resonance peaks are negligibly small.

The effect of translation vibration on damping has not been analyzed much except for two studies by Draminsky [4] and Valev [5]. The experimental investigation by Draminsky found a significant level of damping coming directly from the radial motion between the main journals and bearings. In his work, damping appears to be proportional to the clearance between the main journals and bearings. Based on the finding, Draminsky proposed an empirical formula for estimating the damping coefficient that turns out to be too restrictive for applications to modern reciprocating engines [6]. On the other hand, the

0022-460X/02/$35.00

theoretical analysis by Valev [5] seems to indicate that most of the damping is due to the relative motion between the crank pin and connecting rod. However, no experimental result was given to substantiate the theory.

2. DAMPING MECHANISMS AND MODELLING

Due to the clearances that exist in the joints between the linkages illustrated in Figure 1(a), the kinematic motions are not just simple sliding and rolling types but may also include cyclical lateral and tilting components. For example, joints C, D and E that are basically revolute designs can roll with or without slip and at the same time vibrate transversely as shown in Figures 1(b) and 1(c), while the A and B ones that are of the cylindrical kind can actually slide and simultaneously translate and rotate dynamically normal to the bore axis as depicted in Figures 1(d)–1(f). In the classical rolling motion case, even though the damping effects of pure rolling and pure slipping are difficult to separate out individually, its net vibratory energy dissipation due to simple shear resistance in the oil film can be obtained by performing a perturbation analysis about the mean geometry at a specific crank angle position [1, 2]. Similarly, the effect of sliding perturbation on damping in the lubricated piston and cross-head due to viscous friction was also formulated earlier [1, 2]. However, the fundamental effects of lateral and tilting vibrations were not quantified previously in spite of the appearance that they contribute to the total damping in

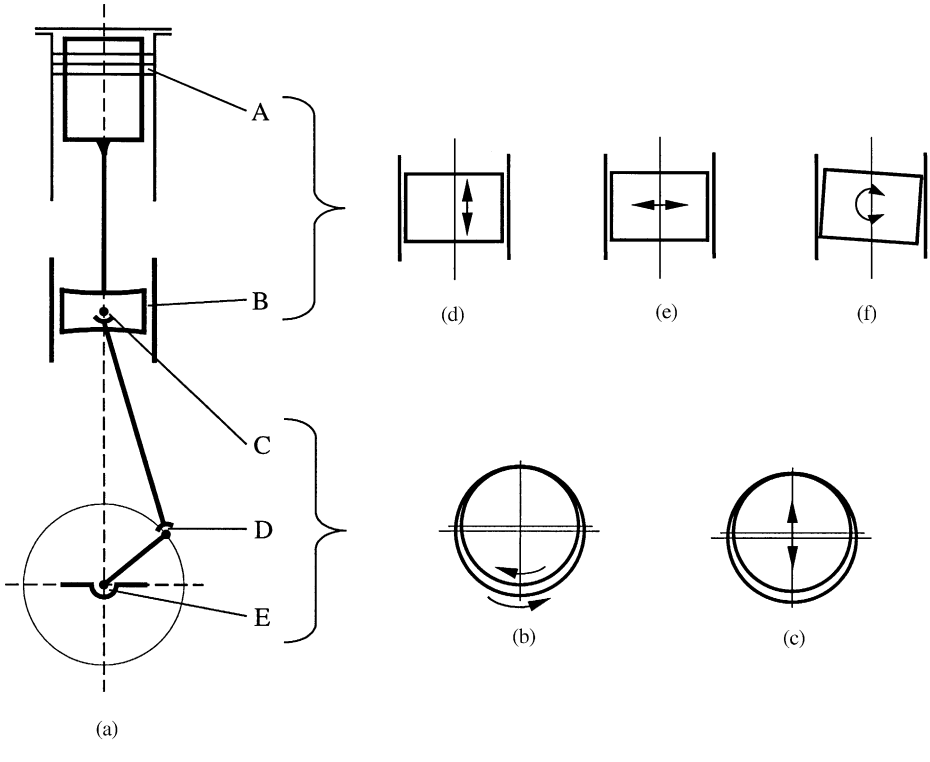

Figure 1. Kinematic motions at the joints of a reciprocating engine: (a) primary linkages include piston–cylinder bore A, cross–head–slide shoe B, connecting rod–cross–head pin C, connecting rod–crank pin D and main journal bearing E; (b) rolling with or without slip; (c) transverse vibration; (d) sliding; (e) normal vibratory motion; (f) rotational vibratory motion.

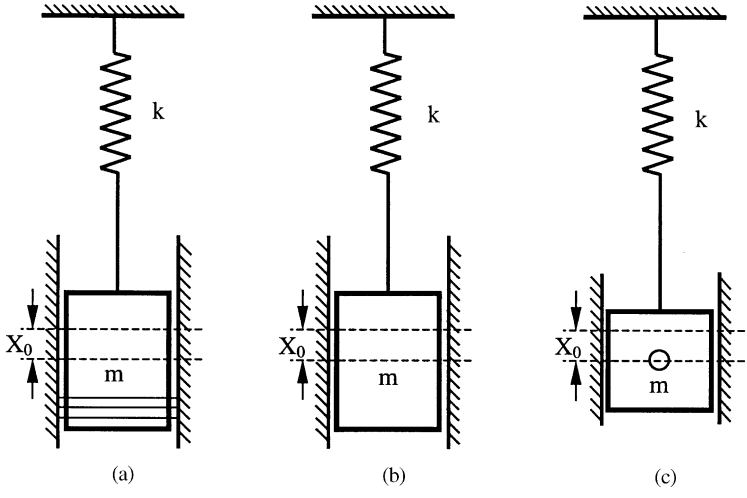

Figure 2. Simple spring–mass system experiments for measuring viscous friction damping of reciprocating parts: (a) piston with rings; (b) piston without rings; (c) cross–head; spring stiffness $k = 1{\cdot}678 \times 10^5$ N/m (piston), $0{\cdot}4194 \times 10^5$ N/m (cross–head); masses $m = 4{\cdot}48$ kg (piston), 1·12 kg (cross–head).

the system possibly through oil film resistance to these types of motions and/or repetitive impacts between joint surfaces. One of the reasons is the less predictable nature of random-like motions. For discussion sake, we will refer to this form of damping as non-friction type.

In order to quantify the damping effect from the lateral and tilting motions, which are difficult to compute or measure directly, we examine the viscous friction damping due to the rolling and sliding mechanisms. The difference between the total damping in each joint and the viscous friction damping yields the non-friction damping from the lateral and tilting vibrations. Note that the total dampings in each joint for quasi-static and operating conditions were obtained in the early study [2].

To determine the viscous friction damping in the joints, two sets of free decaying single–degree-of-freedom oscillatory experiments are set up for the reciprocating and rotating parts as shown in Figures 2 and 3 respectively. The simple spring–mass systems shown in Figure 2 simulate the reciprocating piston and cross-head, while the pendulum test shown in Figure 3 mimics the rotating joints in the connecting rod and crankshaft. The materials and lubricated surfaces in these joints are maintained the same as they exist in the engine setups discussed in the two previous communications by Wank and Lim [1, 2]. For each experimental group, three different cases are examined. Cases (a, b) in Figure 2 are used to obtain the translation damping coefficients of joint A with and without piston rings denoted by C_{fP1} and C'_{fP1} respectively. Case (c) in Figure 2 gives the translation damping coefficient C_{fP2} of joint B. These damping coefficients are obtained by tracking the rate of decay of free oscillations given an initial displacement X_0 from the equilibrium position. Applying the well-known log decrement method [10], the value of damping coefficient C_{fP} of the spring–mass systems can be calculated as

$$C_{fP} = \frac{\sqrt{km}}{\pi N} \ln \frac{X_i}{X_{i+N}}, \tag{1}$$

where k and m are spring stiffness and mass of the vibrating part, and $X_j, j = i, i + N$, is the peak amplitude of the jth cycle of oscillation from rest. Repeating equation (1) numerous

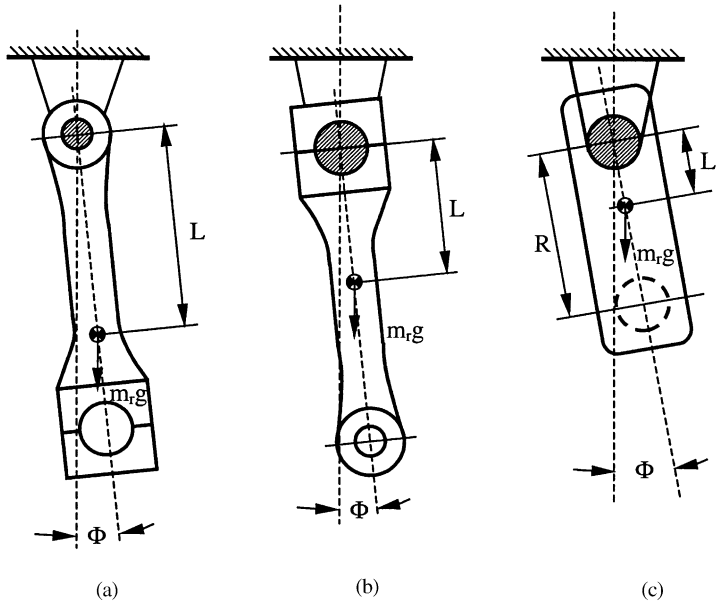

Figure 3. Simple pendulum experiments for measuring viscous friction damping in rotating joints: (a) top end of connecting rod with $L = 0{\cdot}126$ m, $I = 0{\cdot}14026$ kg m^2 and $m_r = 6{\cdot}81$ kg; (b) bottom end of connecting rod with $L = 0{\cdot}112$ m, $I = 0{\cdot}11756$ kg m^2 and $m_r = 6{\cdot}81$ kg; (c) crank shaft and main bearing interface $L = 0{\cdot}029$ m, $I = 0{\cdot}03843$ kg m^2, $R = 0{\cdot}075$ m and $m_r = 16{\cdot}86$ kg.

TABLE 1

Localized viscous friction damping coefficients of reciprocating parts ($\times 10^2$ *N s/m*)

Cases	Parameters	Averages	Variation range
Piston with rings	C_{fP1}	0·2886	0·2922–0·2858
Piston without rings	C'_{fP1}	0·1906	0·1898–0·1915
Cross-head	C_{fP2}	0·1890	0·1876–0·1918

times for the three spring–mass experiments yield the range of values of damping coefficients of C_{fP1}, C'_{fP1} and C_{fP2} given in Table 1. Results shown that C'_{fP1} and C_{fP2} are nearly the same as expected, since both lubricated surfaces are similar. Due to the presence of piston rings, C_{fP1} is found to be higher than C'_{fP1}; an about one-third higher damping level is observed.

For the second group of experiments involving only the revolute joints as shown in Figure 3, three cases to determine the angular damping coefficients $C_{\varphi fR1}$, $C_{\varphi fR2}$, and $C_{\varphi fk}$ at joints C, D and E, respectively, are analyzed. Employing the log decrement method again, equation (1) can be adapted for angular motion to compute the angular damping coefficient C_φ given by

$$C_\varphi = \sqrt{\frac{m_r g L I}{\pi N}} \ln \frac{\Phi_i}{\Phi_{i+N}}, \tag{2}$$

TABLE 2

Localized viscous friction damping coefficients of rotating and rocking parts ($\times 10^{-2}$ *N m s/rad*)

Joints	Parameters	Averages	Variation range
C	$C_{\varphi fR1}$	1·423	1·426–1·421
D	$C_{\varphi fR2}$	1·803	1·796–1·808
E	$C_{\varphi fk}$	1·812	1·809–1·816

where m_r and I are the total mass and mass moment of inertia of the rotating parts, L is the distance from supported joint to the center of gravity, and Φ_j, $j = i$, $i + N$, is the peak angular displacement of the jth cycle of oscillation. Using equation (2), the angular damping coefficient $C_{\varphi fR1}$, $C_{\varphi fR2}$ and $C_{\varphi fk}$ can be determined as listed in Table 2. The experiments reveal that $C_{\varphi fR1}$, $C_{\varphi fR2}$ and $C_{\varphi fk}$ are about the same order of magnitudes with $C_{\varphi fR2}$ and $C_{\varphi fk}$ nearly identical due to their close journal diameters, and $C_{\varphi fR1}$ being the smallest. The damping coefficients $C_{\varphi fR1}$ and $C_{\varphi fR2}$ are further transformed into their equivalent translation forms denoted by C_{fR1} and C_{fR2} by using $C_{fR2} = C_{\varphi fR2}/r_1^2$ and $C_{fR2} = C_{\varphi fR2}/r_2^2$. Here, $r_1 = 27{\cdot}5$ mm and $r_2 = 31$ mm are the radii of the upper and lower revolute joints of the connecting rod. The resultant averaged damping coefficients C_{fR1} and C_{fR2} are $0{\cdot}1882 \times 10^2$ and $0{\cdot}1876 \times 10^2$ N s/m, respectively, which are comparable to C_{fP1} and C_{fP2} in Table 1. That indicates that the viscous friction damping due to oil film shear resistance is not affected much by the nature of the mechanisms, whether it is the rolling or sliding type, in the joints.

Based on the viscous friction damping coefficients obtained above, the damping effect from the lateral and tilting vibrations can now be determined indirectly. Recall from the early note [2] that the crank angle–dependant net-equivalent torsional damping coefficient C_α is given by

$$C_\alpha = C_c + C_{\alpha P1} + C_{\alpha P2} + C_{\alpha R1} + C_{\alpha R2}, \tag{3}$$

where, C_c is the time-invariant crankshaft damping coefficient, and $C_{\alpha P1}$, $C_{\alpha P2}$, $C_{\alpha R1}$ and $C_{\alpha R2}$ are the equivalent torsional damping coefficients for the piston, cross-head and connecting rod upper and lower revolute joints respectively. The latter four damping coefficients can be further expressed as

$$C_{\alpha Pj} = C_{Pj} R^2 [\sin(\alpha) + \lambda \sin(2\alpha)/2]^2, \quad j = 1, 2, \tag{4a, b}$$

$$C_{\alpha R1} = C_{R1} r_1^2 [(\lambda + \lambda^3/8)\cos(\alpha) - \lambda^3 \cos(3\alpha)/8]^2, \tag{4c}$$

$$C_{\alpha R2} = C_{R2} r_2^2 [1 + (\lambda + \lambda^3/8)\cos(\alpha) - \lambda^3 \cos(3\alpha)/8]^2, \tag{4d}$$

where α is the crank angle, R is the crank radial distance as shown in Figure 3(c), and λ is ratio of R to the length of the connecting rod (joint-to-joint distance). Furthermore, the time-averaged damping coefficient is given by

$$C_Z = C_c + C_{ZP1} + C_{ZP2} + C_{ZR1} + C_{ZR2}, \tag{5}$$

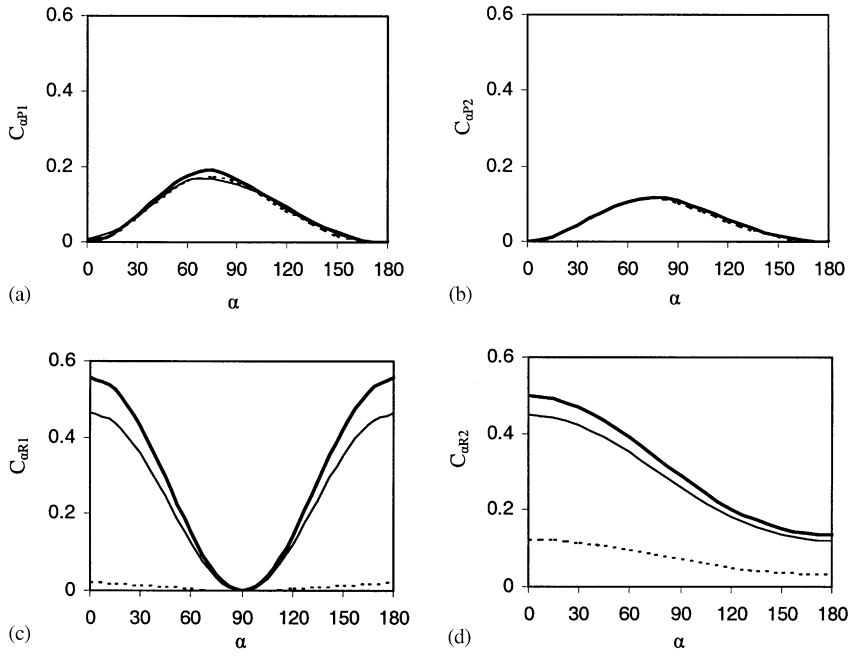

Figure 4. Comparisons of viscous friction and net damping contributions: (a) piston–cylinder bore; (b) cross-head–slide shoe; (c) connecting rod–cross-head pin; (d) connecting rod–crank pin; ——, net damping of mode-1; ——, net damping of mode-2; - - - - -, viscous friction damping coefficients from single–degree-of-freedom free vibration tests.

where the specific time-averaged torsional damping coefficients in the right-hand side are

$$C_{ZPj} = C_{Pj}R^2(1 + \lambda^2/4)/2, \quad j = 1 \text{ or } 2, \tag{6a, b}$$

$$C_{ZR1} = \tfrac{1}{2}C_{R1}r_1^2\lambda^2(1 + \lambda^2/4 + \lambda^4/32), \tag{6c}$$

$$C_{ZR2} = \tfrac{1}{2}C_{R2}r_2^2(2 + \lambda^2 + \lambda^4//4 + \lambda^6/32). \tag{6d}$$

Inserting the localized viscous friction damping coefficients C_{fP1}, C_{fP2}, C_{fR1} and C_{fR2} into equation (4) yields the equivalent torsional damping coefficients shown in Figures [4(a)–4(d)] as dashed line functions. They are compared to two other damping curves that are shown in thin and thick solid lines for net damping levels of torsional modes 1 and 2, respectively, which were obtained from a series of quasi-stationary engine experiments as discussed in reference [2]. From the comparisons of the dashed and solid line curves in Figures 4(a) and 4(b), it is found that the viscous friction contributions make up most of the net dampings seen in reciprocating parts (piston and cross-head). In the case of the rotating joints of the connecting rod given by Figures 4(c) and 4(d), the viscous friction contributions are significantly less than the net damping levels measured. The differences between them are attributed to the damping from the oil film resistance to transverse and tilt motion, and/or impactive behavior, which are substantially higher overall than the levels seen in the reciprocating components. This may be because of the larger clearances in joints C and D resulting in more severe lateral and tilting vibrations.

In the case of the crankshaft, its net-equivalent torsional damping coefficient C_c may come from the viscous friction and non-friction damping in the main journal bearing (C_k), and internal material damping due to hysteresis in the crankshaft (C_h). For a low-speed

TABLE 3

Time-averaged viscous friction, material and non-friction damping proportions in each joint and the complete single-cylinder engine installation. Note that the damping values are expressed in term of the equivalent torsional form

Joints	Viscous friction damping (N m s/rad)	Material damping (N m s/rad)		Non-friction damping (N m s/rad)		Total damping (Nm s/rad)		Non-friction damping contribution (%)	
		Mode-1	Mode-2	Mode-1	Mode-2	Mode-1	Mode-2	Mode-1	Mode-2
A	0·0832	—	—	0·0006	0·0068	0·0838	0·0900	0·7	7·6
B	0·0545	—	—	0·0002	0·0004	0·0547	0·0549	0·3	0·7
C	0·0007	—	—	0·2375	0·2857	0·2382	0·2864	99·7	99·8
D	0·0184	—	—	0·2537	0·2840	0·2721	0·3024	93·2	93·9
E	0·0181	0·1592	0·2914	0·1412	0·2733	0·3185	0·5828	44·3	46·7
Complete engine	0·1749	0·1592	0·2914	0·6332	0·8507	0·9673	1·3165	65·5	64·6

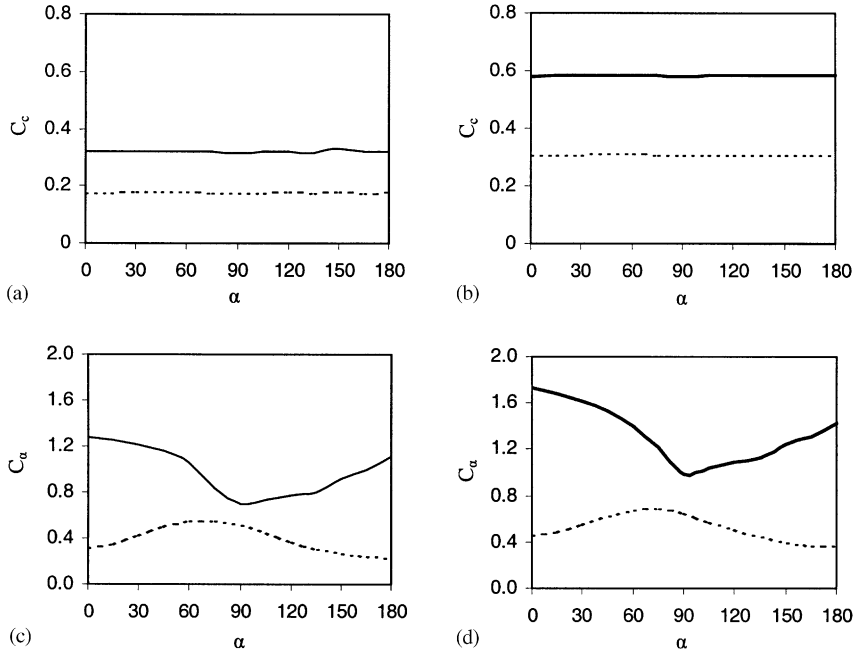

Figure 5. Comparisons of combined viscous friction-material damping and net damping contributions of the main journal bearing and crankshaft for (a) mode 1 and (b) mode 2, and the complete engine for (c) mode 1 and (d) mode 2. Curves: ——, mode-1; ——, mode-2; - - - -, combined viscous friction-material damping.

engine (with cross-head), Iwamoto and Wakabayashi [8] found the hysteretic damping to be about half of C_c, i.e., $C_h \approx C_c/2$. Assuming the same case in our system, C_h can be determined from the crankshaft damping coefficient C_c values of modes 1 and 2 as listed in Table 3. Then, from the result of the Figure 3(c) experiment, the combined viscous friction and material damping coefficients $C_{\varphi fk}$ of the crankshaft for modes 1 and 2 are obtained,

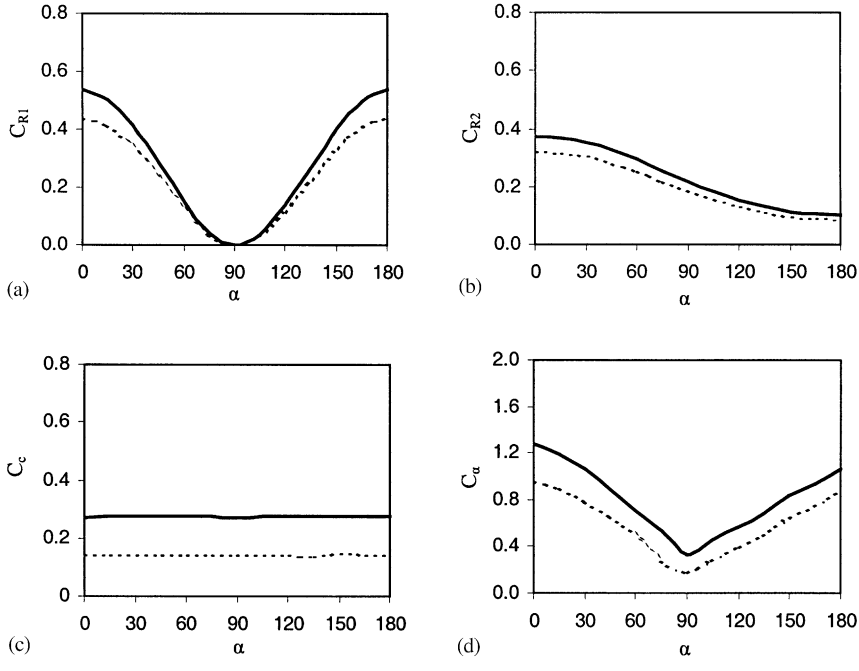

Figure 6. Variation of non-friction damping coefficients: (a) connecting rod–cross-head pin; (b) connecting rod–crank pin; (c) contributions of the main journal bearing and crankshaft; (d) the complete engine; ——, mode-1; - - - -, mode-2.

and shown in Figures 5(a) and 5(b) using dashed lines. Note that the solid line curves are net damping levels from quasi-stationary engine experimental results. It may be pointed out that the dampings are essentially independent of crank angle α. Applying equation (3), the total frictional and material dampings of the complete engine can be calculated and are shown in Figures 5(c) and 5(d) as dashed lines for vibration modes 1 and 2 respectively. In the same figures, the net damping levels of the engine are shown in solid lines. Hence, the non-friction dampings of the revolute joints and the complete engine can be calculated by taking the difference between the solid and dashed line functions in Figures 4 and 5. The results are shown in Figure 6. It may be worth noting that the variation trend seen in Figure 6(d) is quite similar to the solid line curves in Figures 5(c) and 5(d). This suggests that the non-friction damping may be the main contributor to the crank angle variation in the net damping level of the engine.

Substitutions of C_{fP1}, C_{fP2}, C_{fR1} and C_{fR1} into equation (6) yield the corresponding time-averaged torsional damping coefficients of C_{fzP1}, C_{fzP2}, C_{fzR1} and C_{fzR2} due to viscous friction. It follows that C_{fz} can be computed from equation (5). The estimated friction damping coefficients are listed in the second column of Table 3 along with material, non-friction and total damping coefficients. It is obvious that non-friction dampings in the reciprocating parts are very small and negligible, while those in the rotating parts are quite large. In fact, in the two joining ends of the connecting rod, nearly all vibratory energy dissipations come from the effective damping arising from non-friction type damping. For the complete single-cylinder engine, the non-frictional damping due to cyclical lateral and tilting motions accounted for about two-thirds of the net damping, which is clearly quite significant.

3. PARAMETRIC ANALYSIS

The effects of clearances, lubrication oils and materials in the joints on damping coefficients are examined next. These are of interest because of the role they play in stimulating cyclical lateral and tilting motions that give rise to non-frictional (including impactive) damping. A pair of quasi-stationary and operating experiments using the single-cylinder engine system developed previously [1, 2] is utilized here again as shown in Figure 7. Details of the test and measurement setup are already described in the earlier two papers [1, 2]. Like before, the first two flexible system torsional modes are analyzed. Higher order modes are not considered due to the fact that their frequencies are much higher than the rotational speed range used in typical reciprocating engines.

The effect of clearances is considered first. Note that the baseline clearances δ_0 at joints A, B, C, D and E are 0·05, 0·10, 0·12, 0·15 and 0·15 mm respectively. The clearances between the contacting surfaces of A and B are measured using a plug gauge, while the gaps in joints C–E are measured applying a pressed lead strip. In our analysis, the clearances δ in B–E are

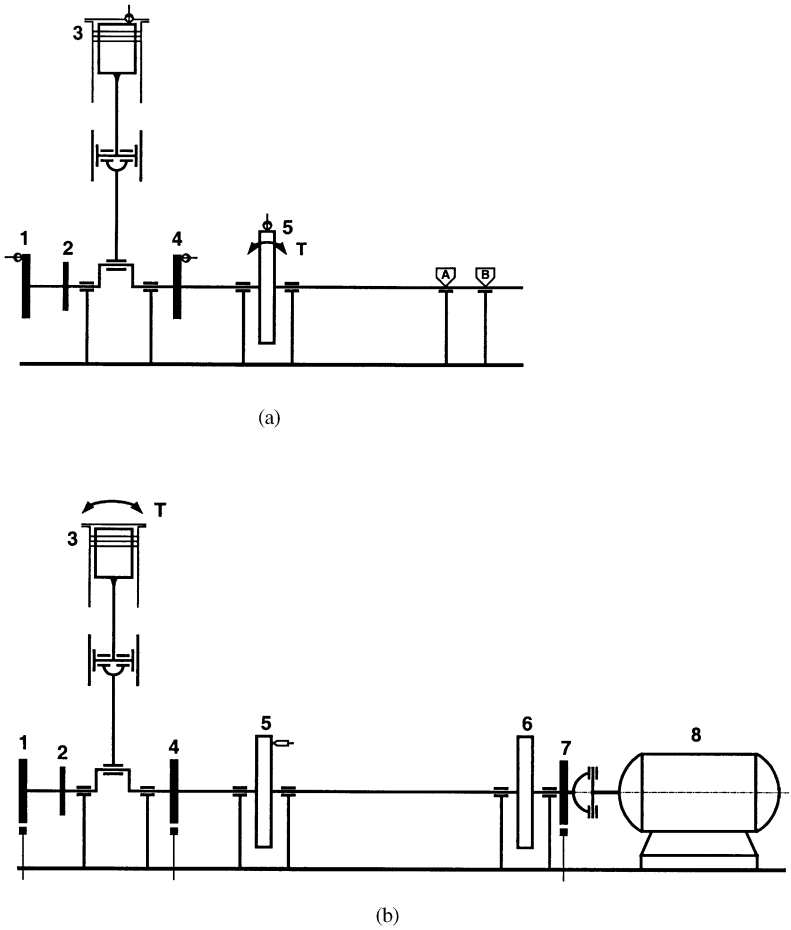

Figure 7. Single-cylinder engine set-up for (a) quasi-stationary and (b) operating test. Labels: 1, measurement gear; 2, attachment disk; 3, cylinder; 4, measurement gear; 5, flywheel; 6, flywheel; 7, universal joint; 8, DC motor; , accelerometers; , fixed nodal point for mode 1; , fixed nodal point for mode 2; T, input torque fluctuation; , magnetic pickup transducer; , tachometer.

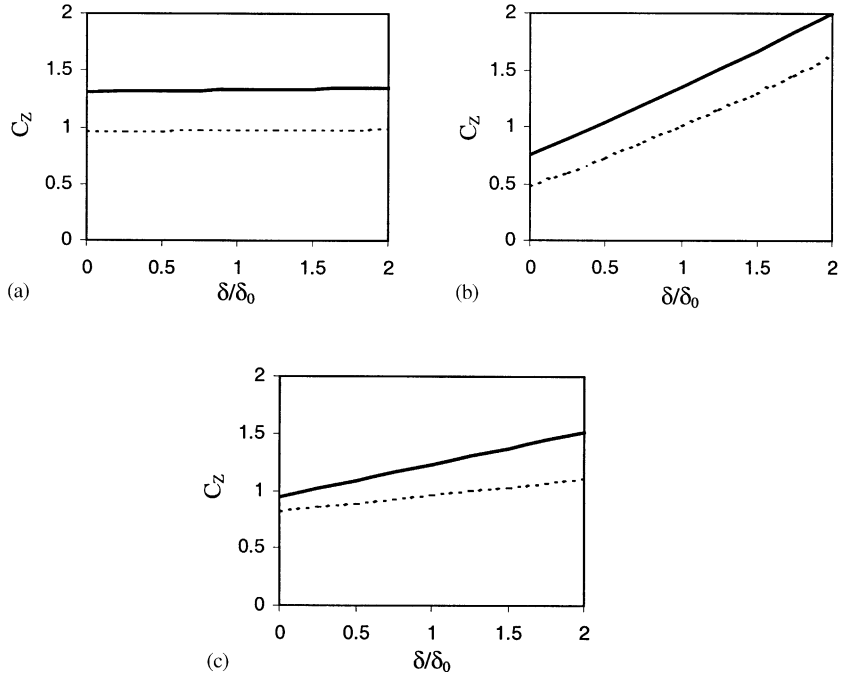

Figure 8. Effect of clearance ratio δ/δ_0 on C_Z based on operating experiments: (a) cross-head–slide shoe clearance; (b) revolute joints in connecting rod; (c) crank shaft-main bearing clearances; ----, mode-1; ——, mode-2.

varied from 25% to 200% of their baseline dimensions. The changes are accomplished using different size shims. Note that the clearance in Joint A is not varied because of interferences from the piston rings and cylinder bore. Repeating the analysis discussed earlier for each new set of δ values, we obtain the results shown in Figure 8. Figure 8(a) gives the time-averaged damping coefficient of the complete engine by varying δ/δ_0 between the cross-head and slide shoe. In this plot, C_Z remains essentially the same, which is consistent with the fact that the level of non-friction damping is small. Figure 8(b) shows the variation of C_Z due to change in the clearances at both ends of connecting rod, and Figure 8(c) plots the variation of C_Z relative to change in the clearances of the main journal bearings. In both case, C_Z increases with increasing δ/δ_0 with the greater rate of increase observed in Figure 8(b). This is because the contribution from non-friction damping is more significant in these joints as shown in Table 3 as well. In summary, the results prove that the non-friction (impactive) damping is mainly contributed by the rotating joints in the reciprocating engine. Therefore, the variation in the net-equivalent torsional damping coefficient C_α as a function of crank angle α should also be affected significantly with modifications made to the clearance in the revolute joints of the connecting rods. This is actually confirmed by the results of the quasi-stationary experiments as shown in Figure 9 for modes 1 and 2.

From the experimental results shown in Table 3, the contribution of viscous friction damping to the total damping of the engine is about one-sixth, which is approximately the same as the contribution from material damping of the crankshaft. These shares are much less than non-friction damping. Therefore, the measured damping should not be sensitive to the frictional conditions such as lubricating oil and material of the parts. To verify this conclusion, two sets of experiments are done. First, the lubricating oil used is changed. The re-computed damping coefficients are given in Table 4, which show little change in C_Z. The

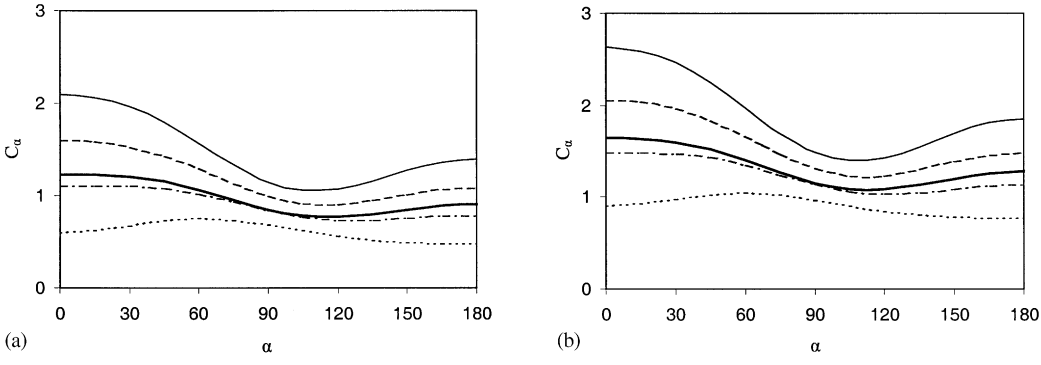

Figure 9. Effect of radial clearance ratio δ/δ_0 at revolute joints of the connecting rod based on quasi-stationary experiments: (a) mode-1, (b) mode-2, ·····, $\delta/\delta_0 = 0{\cdot}25$; –·–·–, $\delta/\delta_0 = 0{\cdot}75$; ——, $\delta/\delta_0 = 1{\cdot}0$; – – – –, $\delta/\delta_0 = 1{\cdot}25$; ——, $\delta/\delta_0 = 1{\cdot}75$.

TABLE 4

Effects of three different types of lubricating oils on C_Z (N m s/rad)

Lubricating oil types	Variation range		Average	
	Mode-1	Mode-2	Mode-1	Mode-2
SAE 20	0·9516–0·9620	1·3011–1·3121	0·9593	1·3071
SAE 30	0·9602–0·9725	1·3103–1·3251	0·9670	1·3163
SAE 40	0·9766–0·9832	1·3178–1·3294	0·9738	1·3254

TABLE 5

Effects of three different materials used in the slide shoe and bearings on both ends of the crank pin on C_Z (N m s/rad)

Material	Variation range		Average	
	Mode-1	Mode-2	Mode-1	Mode-2
ChSnSb11-6	0·9582–0·9636	1·3052–1·3146	0·9603	1·3120
ChSnSb6	0·9638–0·9697	1·3140–1·3192	0·9670	1·3163
AlSnCu	0·9696–0·9753	1·3198–1·3250	0·9718	1·3216

second experiment examines the effect of material. In this study, 3 different types of material are used in the slide shoe and bearings (bushings) on both ends of the crank pin. The corresponding C_Z values are shown in Table 5. Again, it is clear C_Z is insensitive to the type of material employed.

4. CONCLUDING REMARKS

In this communication, the damping in each joint computed in the earlier study is further decomposed into viscous friction, material and non-friction (including impactive) types. The

first two types of damping are well-studied parameters, while the non-friction damping is less known and not well quantified. Our analysis shows that the cyclical lateral and tilting motions are the primary mechanisms responsible for this type of damping. Experimental results indicate that the non-friction damping contribution is very significant and most of them comes from the revolute joints at both ends of the connecting rod. This study also shows that the measured damping levels in the reciprocating engine are sensitive to clearance in the joints of the connecting rod, and are insensitive to the types of lubricating oil and material used.

REFERENCES

1. Y. WANG and T. C. LIM 2000 *Journal of Sound and Vibration* **238**, 710–719. Prediction of torsional damping coefficients in reciprocating engine.
2. Y. WANG and T. C. LIM 2001 *Journal of Sound and Vibration* **242**, 179–193. An analysis of modal damping sources in reciprocating engine.
3. W. KER WILSON 1963 *Practical Solution of Torsional Vibration Problems*, Vol. 2. New York: John Wiley & Sons Inc.
4. P. DRAMINSKY 1948 *Proceedings of the Institution of Mechanical Engineers* **159**, 416–432. Crank Damping.
5. A VALEV 1979 *Proceedings of the* 13*th International Congress of Combustion Engines* (13th *CIMAC*). Relative motion between axis of pin and bore in connecting rod big-end bearings as the most essential damping cause for crankshaft torsional vibrations.
6. Y. WANG, S. T. SONG and X. G. SONG 1996 *Journal of Dalian University of Technology* **36**, 590–594. Comment on empirical formulas for calculating marine engine damping coefficient.
7. E. J. NESTORIDES (editor) (The British Internal Combustion Engine Research Association) 1958. *Handbook on Torsional Vibration*. London: Cambridge University Press.
8. S. IWAMOTO and K. WAKABAYASHI 1985 *Journal of the Marine Engineering Society* **19**, 34–39. A study on the damping characteristics of torsional vibration in diesel engines (Part I).
9. J. F. SHANNON 1935 *Proceedings of the Institution of Mechanical Engineers* **131**, 387–435. Damping influences in torsional oscillation.
10. W. T. THOMSON 1981 *Theory of Vibration with Applications*. Englewood Cliffs, NJ: Prentice-Hall.